

# Refreshing Industrially Processed 6xxx Series Aluminum Alloys after Prolonged Natural Aging

Zi Yang,\* Xichong Zheng, Zeqin Liang, and John Banhart

Natural aging (NA) undesirably hardens 6xxx series aluminum alloys and hampers subsequent paint-bake (PB) hardening, thus limiting the use of material after prolonged storage. It is presented that a refreshment treatment for seconds at a temperature between 230 and 290 °C can effectively lower the hardness/strength of two commercial alloys that have experienced NA for  $\approx 3.5$  years and enhance their PB hardening, thus enabling the reuse of the material with minimal energy input. The treatment is based on dissolving solute clusters formed during prior aging, but precipitation during refreshment can compromise its efficacy. The dependence of cluster dissolution and precipitation on the refreshment parameters as well as on the alloy composition is analyzed. A higher temperature is suggested for refreshing AA6014 alloy than for AA6016 alloy due to a higher thermal stability of the clusters in the former. Natural secondary aging (NSA) is investigated and it is proposed that the remaining undissolved clusters play an important role in controlling the mobile vacancy concentration. Refreshment experiments utilizing various heating media demonstrate that the treatment is hardly sensitive to the heating rate which facilitates its industrial implementation. The refreshed alloy can undergo further preaging to enhance the NSA stability and PB hardening.

casting, homogenization, rolling, solution annealing, quenching, and some preaging (PA) treatment, before the product is shipped to the car manufacturer where it is formed into the desired shape, integrated into the vehicle structure, and eventually paint-baked. During the last procedure strength enhancement takes place derived from the formation of nm-sized precipitates in the matrix, which enables the material to meet the required service strength level and dent resistance. It is therefore demanded that the alloy remains at a low strength level before forming while still retaining a high precipitation hardening potential in artificial aging (AA), which is combined with paint-baking (PB) in the automotive industry. Ideally, one would prefer to reserve all the dissolved solute atoms, primarily Mg and Si, in the solid solution state before PB. In practice, however, this is not feasible as cluster formation (early aggregation of solute atoms) starts already during low-temperature natural aging (NA), i.e., during

storage and transportation, thus hardening the material notably. Another critical issue specifically related to the alloys that contain a combined Mg + Si content higher than  $\approx 1\%$  is the compromised hardening potential in the subsequent PB process, a phenomenon termed ‘negative effect’. Even minutes of NA may already induce a strong “negative effect”.<sup>[2]</sup>

To keep the material “fresh” and resistant to NA, several methods can be applied. Technically the easiest way is to lower the temperature of storage since precipitation is temperature dependent. However, this is certainly not an economical solution, as precipitation can start at temperature as low as  $-40$  °C,<sup>[3]</sup> and the time between solution heat treatment and paint baking can be months or longer. Efforts can also be put to work on the diffusion mechanism of solutes. By adding a trace amount of vacancy-binding elements such as Sn or In<sup>[4–7]</sup> the diffusion of solutes, and thus precipitation can be slowed down. This novel method is rather new and, to the authors’ best knowledge, has not yet been applied in mass production. Industrial practice for suppressing NA makes use of a PA step, which operates at intermediate temperatures, modestly strengthening the alloy without introducing the negative effect.<sup>[8]</sup> However, such methods (both micro-alloying and PA) are not able to fully eliminate the NA problem, but rather delay it, so that within a certain time period, normally 6 months, its effect is controlled to an industrially acceptable extent. In view of the supply chain instabilities experienced recently, some materials might have naturally aged for much


## 1. Introduction

Heat-treatable 6xxx aluminum alloys are utilized in the automotive industry to manufacture lightweight car body panels.<sup>[1]</sup> In the common process chain, the alloy is first produced into sheet coils in the material supplier plant, involving procedures such as

Z. Yang, J. Banhart  
Institute for Applied Materials  
Helmholtz-Center Berlin for Materials and Energy  
Hahn-Meitner-Platz 1, 14109 Berlin, Germany  
E-mail: zi.yang@helmholtz-berlin.de

X. Zheng, J. Banhart  
Materials Science and Technology  
Technical University Berlin  
Hardenbergstraße 36, 10623 Berlin, Germany

Z. Liang  
Novelis R&T Centre Sierre  
Route des Laminoirs 15, 3960 Sierre, Switzerland

 The ORCID identification number(s) for the author(s) of this article can be found under <https://doi.org/10.1002/adem.202301102>.

© 2023 The Authors. Advanced Engineering Materials published by Wiley-VCH GmbH. This is an open access article under the terms of the Creative Commons Attribution License, which permits use, distribution and reproduction in any medium, provided the original work is properly cited.

DOI: 10.1002/adem.202301102

longer than 6 months, and properties have deteriorated so that processing requirements are not met anymore. Finding a solution to treat these “expired” alloys is therefore highly desirable. Recycling these materials back to casting or solution heat treatment is an option, but such steps require high-temperature processing that is energetically and economically not favorable.

It is well-known that the clusters formed during NA can be dissolved at elevated temperatures,<sup>[9–11]</sup> which provide another opportunity to refresh the material after prolonged NA, namely by performing a short reversion aging treatment.<sup>[9,12,13]</sup> This refreshing strategy is potentially advantageous in that the temperature required is much lower than for melting or solution annealing, thus significantly reducing the energy required and the associated CO<sub>2</sub> footprint. However, several scientific and engineering questions still remain about its usage in reality. A major question arises from the different aging histories of the commercial alloys and the alloys presented in the literature. Literature studies usually apply only NA for short times, maximum weeks, to investigate the dissolution of the NA clusters, while the expired alloys in reality have experienced industrial PA and at least 6 months of NA, where the clustering state can be different. It is still unclear if these clusters can be successfully reverted. Moreover, precipitates can form in parallel at such temperatures, but they are generally undesired due to their low hardening effect. This has to be taken into account when finding the right processing window. Furthermore, since the alloys are aimed to be reused in the normal production chain after the refreshing treatment, their stability during natural secondary aging (NSA) and hardenability during PB need to be assessed too.

To address the aforementioned questions, we systematically carried out a variety of refreshment treatments at various temperatures and times to investigate their influences on the reversion of clusters and the improvement of PB hardenability. We also examined the dependence of the NSA stability on the refreshment parameters. Additionally, the wide applicability of the treatment was assessed by applying it to two alloys with markedly distinct compositions. To cope with the reported very short times needed for reversion, the rate of heating to the reversion temperature is important, which is why we also studied the impact of the heating rate on the refreshment process.

## 2. Experimental Section

### 2.1. Material

Refreshment was investigated on two commonly used commercial alloys, namely, AA6014 and AA6016, which have very different Mg and Si contents, as shown in **Table 1**. One-millimeter-thick alloy

**Table 1.** Chemical compositions of the alloys in weight percent. Asterisks (\*) indicates the “fresh” alloys used as references.

Alloy	[Mg]	Si	Fe	Mn	Cu	Al
6016	0.273	1.268	0.165	0.077	0.112	Balance
6016*	0.295	1.303	0.169	0.084	0.120	Balance
6014	0.633	0.584	0.179	0.072	0.129	Balance
6014*	0.655	0.617	0.204	0.093	0.134	Balance

sheets were produced by Novelis, Switzerland. They were industrially solutionized and preaged in a continuous annealing solution heat-treatment line and, by the time of refreshing treatment, had been naturally aging for about 3.5 years. To evaluate the effect of refreshment, two “fresh” alloys were also examined. They had identical processing histories as the refreshed material but had been naturally aged just for a short time (1–2 months) at the time of measurement. Their solute contents are slightly higher than the “expired” alloys, but such small differences are considered to have no pronounced impact on their properties.

### 2.2. Heat Treatments

**Figure 1** schematically describes the heat treatments on the alloys. After prolonged NA for  $\approx 3.5$  years, refreshment (or reversion) aging (RA) was conducted on alloys isothermally at various temperatures from 230 to 290 °C for various times. A liquid metal (“LM”) bath of the low-melting Bi57Sn43 alloy was employed for practicing most of the RA, and only when the effect of heating rate was studied, the other heating media were used, including (from fast to slow heating): 1) a molten salt (“MS”) bath containing a mixture of KNO<sub>3</sub>, NaNO<sub>2</sub>, and Na<sub>2</sub>NO<sub>3</sub>; 2) a silicone oil bath (“OB”); 3) ceramic heating plates (“HP”). In “LM”, “MS”, and “OB”, the media were preheated to the target temperature, i.e., 250 °C, and the samples were held using a thin stiff metal wire and kept in motion in the media, which intends to minimize local cooling of the media due to the heat content of the sample. For refreshment with “HP”, the sample was first placed between the two cold heating plates, as described in the study of Yang et al.<sup>[14]</sup> before it was heated up to the target temperature and held there. Two heating rates (“HP1” and “HP2”) were applied. The temperatures of the sample in various media were measured using the same setup, as described in the study of Madanat et al.<sup>[11]</sup> and the corresponding heating curves are shown in **Figure 1**, from which the average heating rates from 20 to 240 °C are calculated to be  $\approx 220, 88, 31.5, 4.8, 2.5$  Ks<sup>-1</sup> for “LM”, “MS”, “OB”, “HP1”, and “HP2”, respectively.

After refreshment, some samples were further subjected to various aging treatments such as PA, NSA, AA, and various combinations thereof. PA was performed for 20 h in an OB held at 80 °C, while NSA was conducted in a Peltier-cooled incubator held at 20 °C for various times up to 6 months. AA was carried out for 20 min in an OB held at 185 °C, which is also denoted PB in this study. As a notation, we use “RA $x$ / $y$ ” to denote the refreshment at  $x$  °C for a duration of  $y$  seconds (or just RA  $x$  if time is not specified), and “NSA $z$ ” to represent NSA for  $z$  days. For instance, RA230/10 + PA + NSA180 + PB stands for the sample after RA at 230 °C for 10 s, PA at 80 °C for 20 h, NSA for 180 d (6 months), and eventually PB.

Apart from the heat treatments shown in **Figure 1**, the expired alloys were also resolutionized at 540 °C in an air circulation furnace for 1 h and subsequently quenched in ice-water. This state is named as-quenched (AQ). When the AQ sample is further subjected to PB, the intermediate delay time at room temperature is shorter than 30 s.

### 2.3. Methods

Hardness measurement was used as the main method to characterize the aging response of the material due to the simplicity

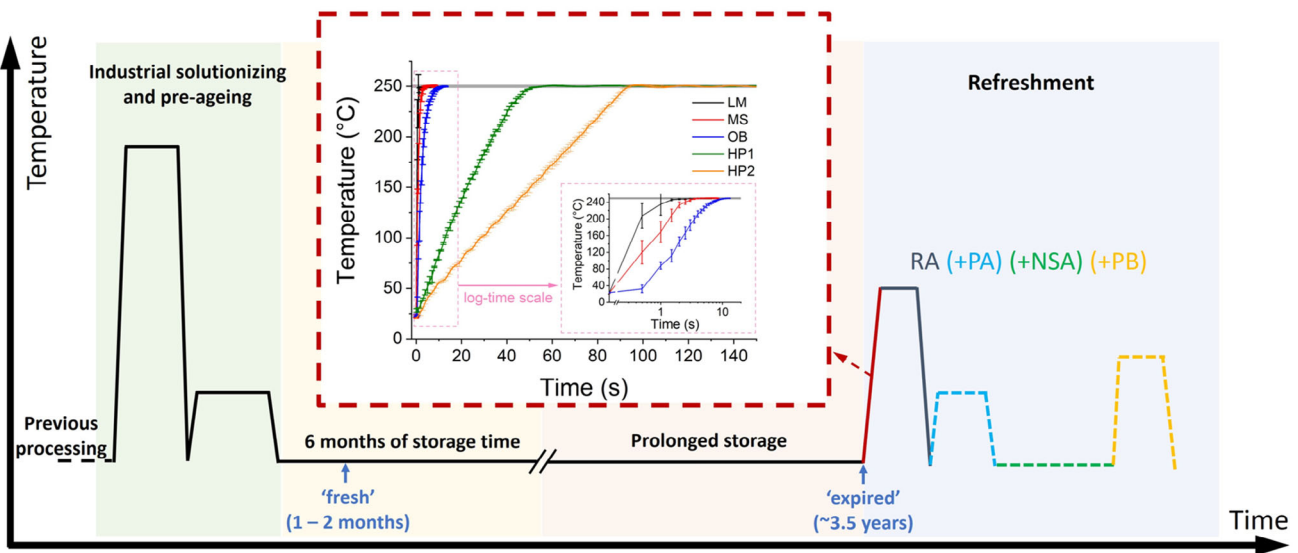


**Figure 1.** Schematic plot of heat treatments of the alloys. The inset shows the sample temperature courses during RA at 250 °C in various media: LM, MS, OB, and heating plate (HP1 and HP2). Each curve represents the average of at least five repeated measurements.

of the measurements. It was performed on a Qness M60 unit applying the Brinell method, a load of 10 kgf (98.1 N), and an indenter of 1 mm diameter. Each measurement consisted of eight indentations, from which the average and standard deviation were calculated.

Tensile testing was performed on the selected alloy (AA6016) and aging states using an Instron 4505 testing machine. The testing procedure was carried out in accordance with the ASTM-E8M standard using the subsize sample geometry. Yield properties were obtained at a strain rate of  $2.5 \times 10^{-4} \text{ s}^{-1}$ , after which the strain rate was enhanced to  $2 \times 10^{-3} \text{ s}^{-1}$  for determining the ultimate tensile strength and uniform elongation. An extensometer was employed for measuring the strain. Each test was repeated at least once for verification of reproducibility. The purpose of these tests was to check whether hardness measurements reflect the course of aging in the same way as tensile properties and to allow for a comparison with industrial minimum required values.

Differential scanning calorimetry (DSC) was used to characterize the alloys in the expired state and after refreshment. The measurements were carried out in a Netzsch 204F1 Phoenix calorimeter. Various heating rates from 3 to  $200 \text{ K min}^{-1}$  were applied in the measurements of the expired alloys, while only  $10 \text{ K min}^{-1}$  was applied in measuring the refreshed samples. Measurements were taken from 0 to  $450 \text{ °C}$  for low heating rates ( $<50 \text{ K min}^{-1}$ ) and from  $-20 \text{ °C}$  for higher heating rates. An immediate rerun after cooling at  $10 \text{ K min}^{-1}$  to the start temperature was used for the baseline correction.

## 3. Results

### 3.1. Hardness Tests

#### 3.1.1. Reference States without Refreshment

Hardness values of both alloys in the three reference states, namely, industrially processed alloy in “fresh” state ( $H_{\text{fresh}}$ ), after

$\approx 3.5$  years of NA ( $H_{\text{expired}}$ ), after resolutionizing and quenching ( $H_{\text{AQ}}$ ), as well as the hardnesses after further PB on these states, are shown in **Figure 2a,b**. It is observed that the hardnesses of the alloys in the AQ state are quite similar, while the  $H_{\text{fresh}}$  and  $H_{\text{expired}}$  are obviously higher for alloy AA6014 than for AA6016. A notable hardness increase is seen from the “fresh” to “expired” state, with  $H_{\text{expired}} - H_{\text{fresh}}$  equal to 16 HBW for alloy AA6014 and 4 HBW for AA6016. The effects of such prolonged NA on subsequent PB for the two alloys are quite distinct. Hardness after further PB treatment (hereafter abbreviated as PB hardness) is notably compromised in alloy AA6016 when the material is subjected to prolonged NA, whereas the PB hardness values of the “fresh” and “expired” states are almost identical in alloy AA6014. In both alloys, the PB hardness of the “fresh” and “expired” states are significantly lower than the PB hardness of the AQ state (gray broken line).

#### 3.1.2. Refreshment

**Influence of Aging Temperature:** A general trend of hardness evolution during isothermal RA at various temperatures is that it first decreases and then increases again. The lowest hardness during RA is observed at an earlier RA time as the aging temperature increases, and the maximum hardness reversion becomes also larger, i.e., from  $\approx 14 \text{ HBW}$  at  $230 \text{ °C}$  to  $\approx 22 \text{ HBW}$  at  $270 \text{ °C}$  in AA6016, and from  $\approx 9 \text{ HBW}$  at  $230 \text{ °C}$  to  $\approx 28 \text{ HBW}$  at  $290 \text{ °C}$  in AA6014. Since the initial hardness values of the two alloys in the “expired” state are different, we use the relative hardness reversion, which can be calculated as  $\frac{H_{\text{expired}} - H_{\text{fresh}}}{H_{\text{expired}} - H_{\text{AQ}}}$ , instead of the absolute hardness reversion for evaluating the effect of RA in the two alloys (Figure 2c). The same RA treatment gives rise to a markedly higher relative hardness reversion in AA6016 than in alloy AA6014. In alloy AA6016, RA at  $270 \text{ °C}$  for 5–10 s brings the hardness almost down to the AQ state ( $\approx 95\%$  relative hardness reversion). Furthermore, it is

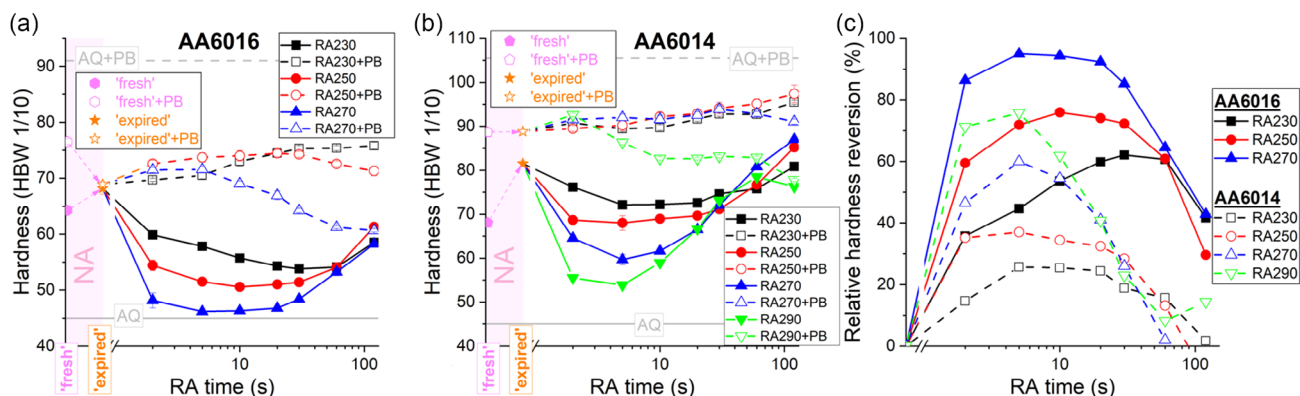


**Figure 2.** Hardness of alloy a) AA6016 and b) AA6014 in various heat-treated states (RA in LM). c) Relative hardness reversion of the alloys during RA as a function of time.

found that in any RA hardness curve, the most substantial reversion is achieved in the shortest time applied (2 s), which accounts for more than half of the maximum hardness reversion.

PB hardness after RA treatment first increases as RA gets longer. A peak in the PB hardness can be observed for RA at 250 °C or higher in AA6016, and RA at 270 °C or higher in AA6014, but not for others within the measured RA time. The highest PB hardness achieved increases as the RA temperature is reduced but is still always much lower than the direct PB hardness of the AQ state (gray broken line). No direct correlation is found between hardness evolution after RA and after ensuing PB. A decrease of RA hardness can correspond to an enhancement of PB hardness (e.g., AA6016, RA at 250 °C from 0 to 5 s), to a rather stable PB hardness (AA6016, RA at 230 °C from 0 to 5 s) or even to a decline in PB hardness (AA6014, RA at 290 °C from 2 to 5 s).

*Influence of Heating Rate:* When heating to the RA temperature is done at a lower rate, hardness evolutions during RA as well as after further PB are delayed, the extent of which are found to be roughly the differences in time needed to reach the RA

temperature (Figure 3). The minimum of the hardness during RA as well as the maximum of the PB hardness are comparable for various heating rates. Only a slight tendency of an increasing minimum hardness can be observed in the RA hardness curves from “LM” to “HP2” (broken lines).

### 3.1.3. NSA Behavior of Refreshed Alloys

Alloys after refreshment gradually go through NSA. Hardening during this process strongly depends on the refreshment parameters, i.e., temperature and time, as well as the alloy type (Figure 4). For instance, AA6016 after RA at 270 °C for 10 s exhibits already a hardness growth of  $\approx 10$  HBW within 1 day of NSA, while AA6014 after RA at 270 °C for 10 s shows a first hardness increase just after 7 days and AA6014 after RA at 230 °C for 10 s barely sees any hardness change for 6 months. Generally, after the same refreshment treatment, alloy AA6016 appears less stable than AA6014, as shown by an earlier commencement of hardening during NSA. In both alloys, RA at a higher temperature for the same time (10 s or 30 s) normally results in stronger NSA. A longer time at the same RA temperature, however, can result in

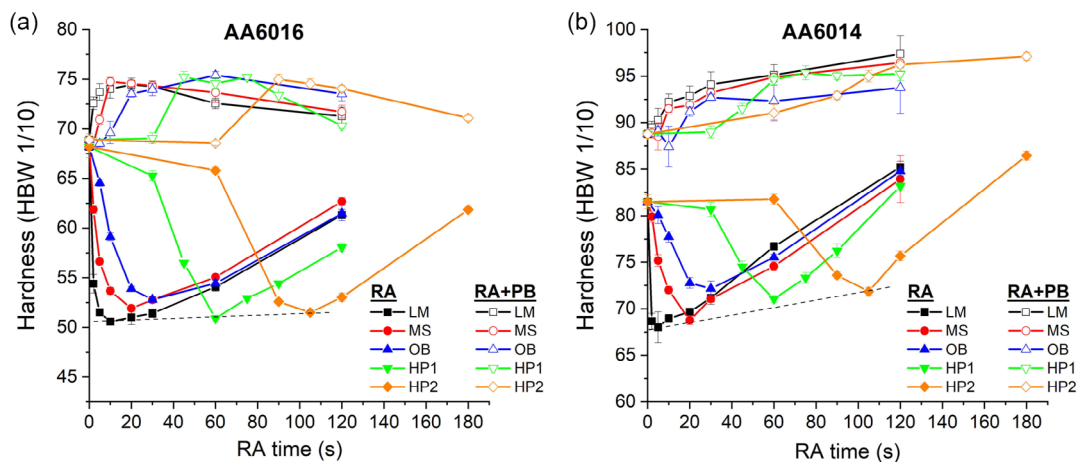


**Figure 3.** Hardness of alloy a) AA6016 and b) AA6014 after RA in various media and thus different heating rates up to the RA temperature (see Figure 1) as well as after subsequent PB.

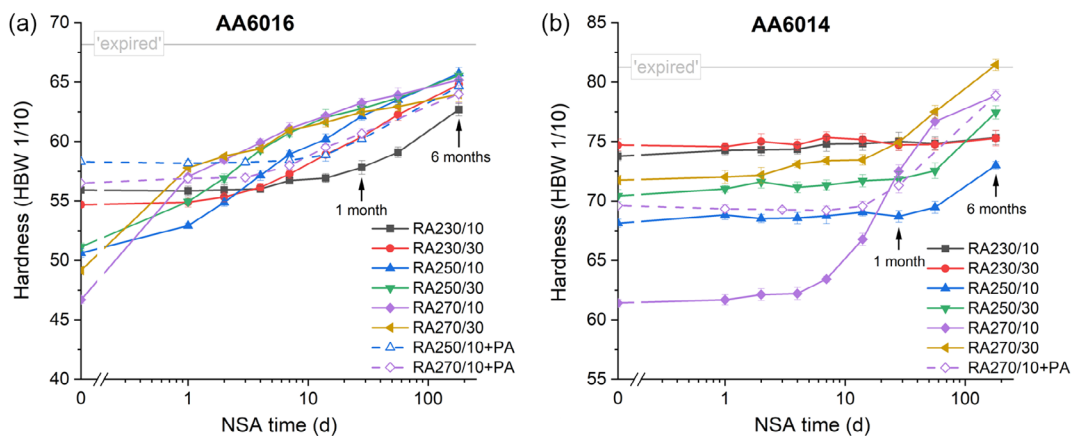


**Figure 4.** Hardness evolution of alloy a) AA6016 and b) AA6014 during NSA after various RA treatments (in LM, solid curves). Selected RA conditions have been further preaged before NSA (dashed curves).

an enhanced NSA stability (e.g., RA270 series in AA6014) or worsen it (e.g., RA230 series in AA6016).

**Figure 5** displays hardness values of the alloys after more RA treatments and additional  $\approx 50$  days of NSA. The hardness increment during such NSA steadily grows in AA6016 when RA time at 230 °C is increased from 5 to 30 s. Longer RA at 250 °C first enhances the hardness increment and later reduces it. The strongest hardening during the measured NSA time is caused by RA at 270 °C but the effect becomes weaker as the RA time is prolonged. This trend is also observed in AA6014 after RA at 270 °C for a longer time, but the overall NSA hardening is less. NSA for 50 days induces only marginal hardness growth in AA6014 after RA at 230 and 250 °C for various times, which agrees well with **Figure 4b** that the alloy is quite stable after RA at lower temperatures.

The influence of NSA on the subsequent PB hardness depends predominantly on the alloy type (**Figure 6**). In AA6016, NSA compromises the PB hardness obviously after just a month of NSA (**Figure 6a,b**). After NSA for 6 months, a drop of 4 and 5 HBW in PB hardness compared to the state without NSA can be observed in samples RA250/10 and RA270/10, respectively. In contrast, PB hardness of the refreshed AA6014 is hardly

influenced by the same intermediate NSA for up to 6 months although a notable hardening has taken place due to NSA (**Figure 6d,e**).

### 3.1.4. Effect of Additional PA on Refreshed Alloys

An additional PA has two effects on the refreshed material. **Figure 4** compares NSA hardening curves of three RA states with and without PA applied. It is obvious that the onset of the hardness increase is delayed, i.e., the stability of the alloy is enhanced. The initial hardness value of the alloy with PA is higher than that without PA because of the extra hardening during PA. However, this relationship is reversed within 1 month of NSA for refreshed AA6014 (RA270/10 with or without PA) and even sooner for refreshed AA6016 series, due to a more rapid hardening of the samples without PA. This beneficial effect of PA lasts for at least 6 months of NSA.

The refreshed samples with PA exhibit also improved PB hardness compared with the ones without PA (**Figure 6c,f**). This applies to the samples directly after RA or after NSA. Moreover, the reduction of PB hardness (in AA6016) caused

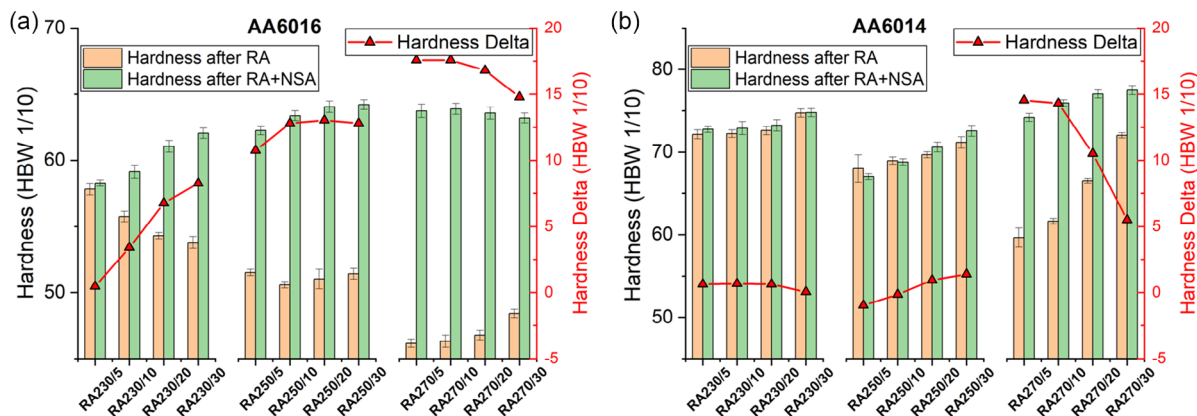


**Figure 5.** Hardness of alloy a) AA6016 and b) AA6014 after corresponding RA (in LM, orange) and subsequent NSA for  $\approx 50$  days (green), as well as the hardness difference of the two states (red curve).

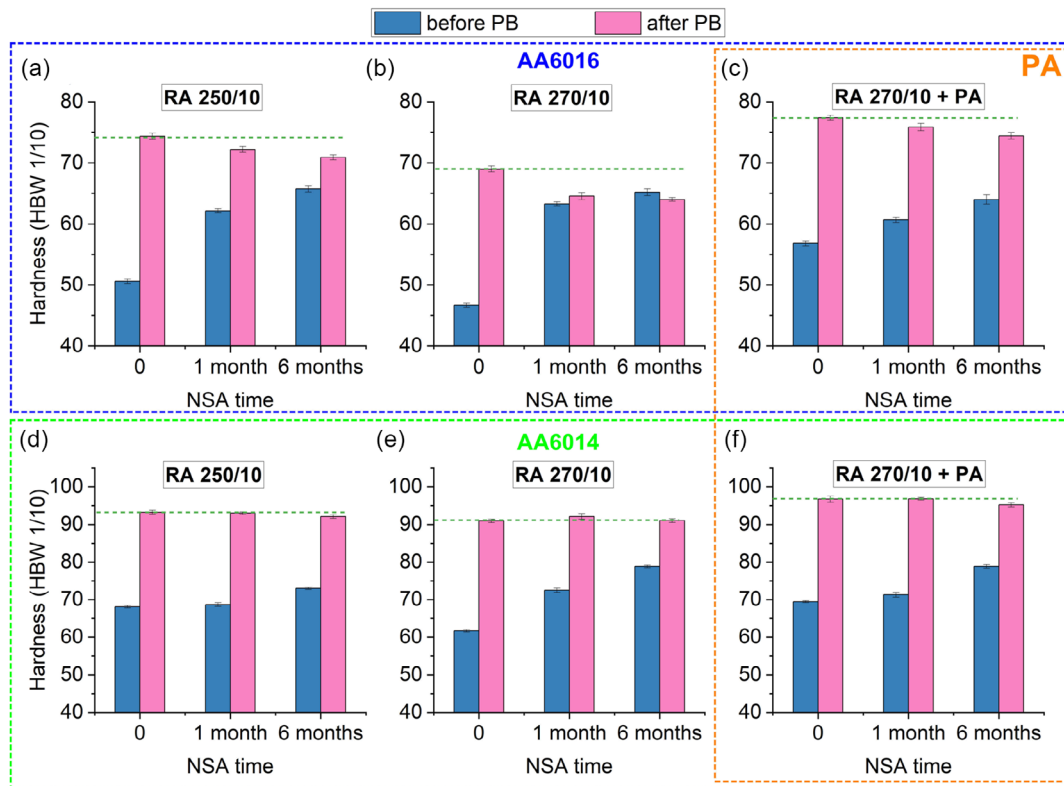


**Figure 6.** Hardness of the refreshed and preaged (only c,f) alloys (heat treatment denoted in the box) after a certain NSA time and after subsequent PB. a–c) AA6016. d–f) AA6014.

by NSA becomes smaller when the alloy has experienced PA due to the suppressed NSA hardening. Therefore, PA treatment after refreshment can simultaneously enhance the stability of the alloy during NSA as well as the PB hardening.

### 3.2. Tensile Tests

**Figure 7** displays the engineering stress–strain curves of the selected states in AA6016. The corresponding properties are listed in **Table 2**. The tests were intended to verify the findings obtained by the hardness measurements but are not as complete as the hardness measurements in terms of the number of heat treatments and alloys. From these tests, it follows that the “expired” sample hardly gains any improvement in yield strength ( $R_{p0.2}$ ) during subsequent PB ( $\Delta=7$  MPa). By applying RA at 270 °C for 10 s, a significant yield strength reduction of  $\approx 54$  MPa is achieved. Subsequent NSA for 1 month strengthens the alloy by more than 40 MPa, but with prior PA, this can be largely reduced to only 6 MPa. PA also removes the serrations visible in the stress–strain curve of the RA sample. Eventually, a PB response of 52 MPa is obtained in the refreshed alloy with additional PA and NSA for 1 month, which is 45 MPa higher than the PB response without refreshment. All these findings agree very well with the hardness data, which justify the usage of hardness measurements for a rapid assessment of the refreshment effect. By plotting the yield strengths of the samples as a function of their hardness values, a linear approximation can be

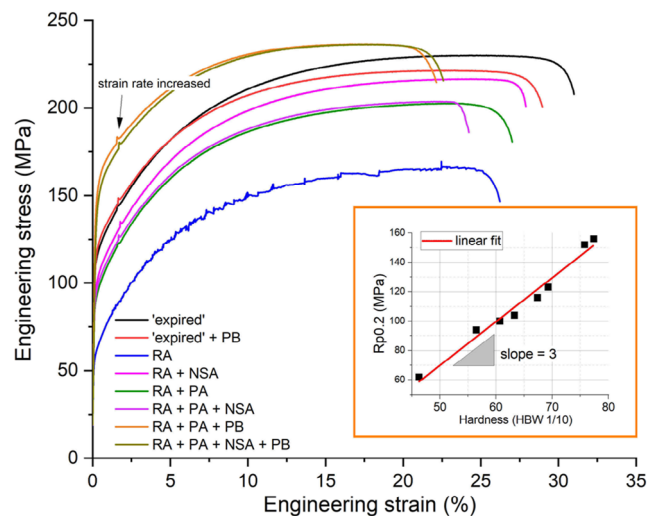


**Figure 7.** Engineering stress–strain curves of alloy AA6016 in various heat treatment states. RA represents RA270/10, and NSA is 1 month. The inset shows  $R_{p0.2}$  plotted as a function of hardness for these states.

established, with a ratio of  $\approx 3$  found in the strength-to-hardness increments, which can be used to estimate strength changes from hardness measurements. What cannot be drawn from the hardness measurement is the elongation information which is also important for evaluating the ductility. The results of the

**Table 2.** Summary of the mechanical properties of the alloy AA6016 in various heat-treated states.

Heat treatment	$R_{p0.2}$ [MPa]	$R_m$ [MPa]	$A_g$ [%]
“expired”	116	230	24.4
“expired” + PB	123	223	22.6
RA	62	168	22.2
RA + NSA	104	217	24.3
RA + PA	94	203	22.8
RA + PA + NSA	100	206	22.7
RA + PA + PB	156	238	17.1
RA + PA + NSA + PB	152	237	15.4

states without PB in Table 2 show that the introduction of RA results in a slight reduction in the uniform elongation ( $A_g$ ), which is still higher than 20%.

### 3.3. DSC

#### 3.3.1. “Expired” Alloys

**Figure 8a,b** shows DSC traces of the “expired” alloys at various heating rates. The exact DSC signals of the two alloys differ from each other but the general courses are analogous. At the slowest measured heating rate (3 K min<sup>-1</sup>), a weak exothermic peak (1) is found in the trace, which is followed by a shallow endothermic trough (2). The trace subsequently sees a major exothermic peak (3), which might be a complex of several peaks since some features can be observed on it, especially for AA6016. As the heating rate is increased, the whole curve shifts to higher temperatures. Moreover, peak (1) gradually shrinks, and the endothermic trough (2) is enlarged. Peak (3) also gets lower as the heating rate is higher.

#### 3.3.2. After Refreshment

DSC curves of the refreshed alloys are measured only at 10 K min<sup>-1</sup> (**Figure 9a,c**). After refreshment for a short time, the endothermic trough (2) gradually disappears and, at a similar position, an exothermic signal emerges. Such exothermic signal

is more pronounced as RA is performed longer or at a higher temperature. As RA further progresses, this trend is reversed and the peak shrinks. Peak (3) is generally lowered as RA proceeds, but it appears that mainly the low-temperature part of the peak is impacted, while the high-temperature part is even slightly enhanced.

The influence of RA on the DSC signal can be observed more clearly when the reference “expired” curve is subtracted. The resulting curves are shown in **Figure 9b,d**, where the major changes can be identified as two peaks, namely *a* and *b*. Peak *a* is exothermic and is first enhanced and later suppressed as RA time is increased. In contrast, peak *b* is endothermic and monotonically decreasing with progressing RA except for some individual cases which can be attributed to the imperfect baseline correction as evidenced by the offsets of the curves at temperatures higher than 300 °C. The maximum magnitudes of peaks *a* and *b* increase as RA temperature rises.

## 4. Discussion

### 4.1. States before Refreshment

The alloys used in this study differ from those used in the literature mainly in that the material has experienced the entire industrial processing history and long NA storage ( $\approx 3.5$  years). Industrial quenching after solutionizing is much slower than water quenching under lab conditions and can lead to some precipitation and lower solute supersaturation (s.s.) after quenching.<sup>[15]</sup> It was found that cooling at various rates results in very similar hardness values in the AQ state of the current AA6014 alloy and others, with a small deviation of only a few hardness units.<sup>[16–18]</sup> This suggests that the hardness in our AQ (resolutionized) state can approximate the hardness after industrial quenching. Consequently, the hardness discrepancy between AQ and “fresh” states can be primarily attributed to the clusters formed during industrial PA, and the hardness between “fresh” and “expired” states to the clustering during prolonged NA storage (see **Figure 2a,b**).

The PB hardness of the “fresh” or “expired” states is significantly lower than that of the AQ state, which could be mainly due to a reduced s.s. after industrial quenching<sup>[15,19]</sup> and clustering during NA that further compromises the PB hardening.<sup>[20]</sup> The latter shows some difference between the two alloys: the

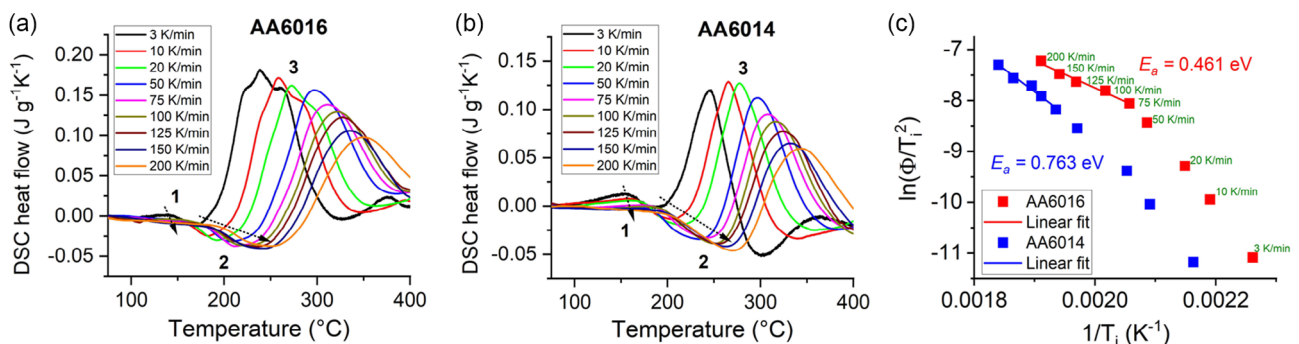


**Figure 8.** DSC traces of the “expired” a) AA6016 and b) AA6014 alloys heated at various rates. c) Kissinger’s activation energy analysis of the endothermic peak (2) in (a) and (b). Linear fitting is applied to the data representing the highest heating rates.

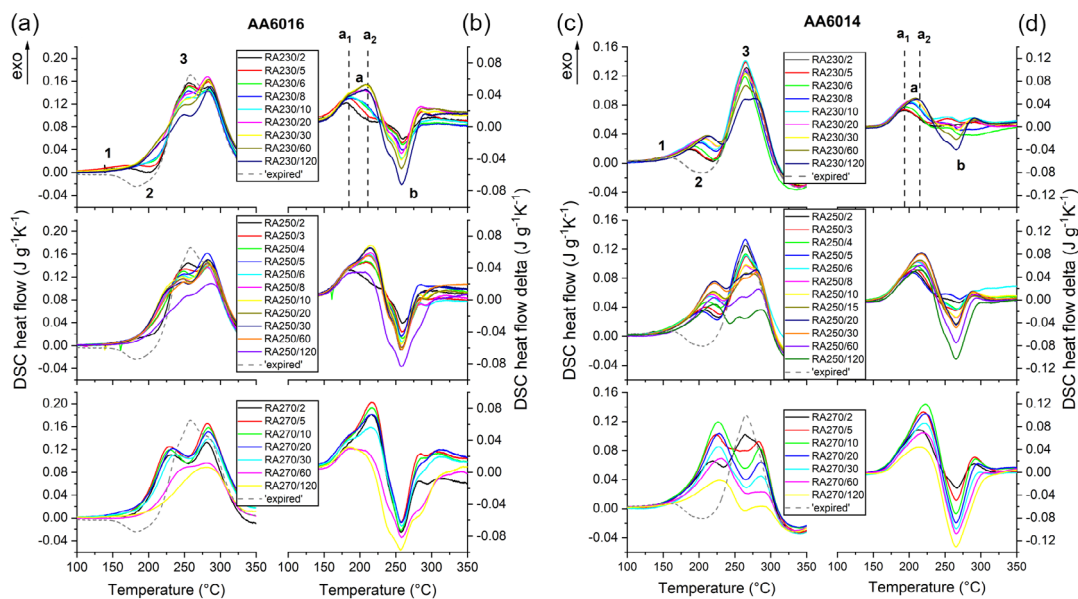


**Figure 9.** DSC traces measured after performing various RA treatments on alloy a) AA6016 and c) 6014. Dashed curves are the reference DSC traces without RA. The differences in DSC traces before and after RA in (a, c) are shown in (b, d).

prolonged NA from “fresh” to “expired” state notably reduces the PB hardness in AA6016, whereas in AA6014 only minimal change is seen (Figure 2a vs 2b). This implies that AA6014 is inherently more resistant to the “negative effect” of NA.

## 4.2. Processes during Refreshment

The hardness progression during RA depicted in Figure 2 is a well-documented phenomenon in the literature<sup>[10,11,13,21]</sup> and comprises two stages. In the first seconds, hardness experiences a sharp decrease, which is attributed to pronounced cluster dissolution. After a transition period of only slowly varying minimal hardness, an ensuing growth stage is caused by the formation of new hardening precipitates. The hardness minimum can be viewed as the outcome of partial compensation of cluster dissolution and precipitation. Our aim is to elucidate how these two processes during RA are influenced by variables such as the RA temperature and time, as well as the alloy composition.

### 4.2.1. Cluster Dissolution

Dissolution of clusters is crucial since it reduces the undesired hardening caused by clusters and also partially reverts the accompanied negative effect, i.e., it facilitates AA. Hardness curves during RA are highly dependent on the RA temperature and as the aging temperature rises minimum hardness decreases (Figure 2). This can be explained by a higher rate of dissolution at increased temperature.<sup>[22]</sup> Comparatively increased dissolution compared to precipitation at a higher temperature can be also derived from the DSC traces at various heating rates (Figure 8). The DSC signal is a complex superposition of precipitation (exothermic) and dissolution (endothermic) reactions. As the heating rate is enhanced, the entire DSC curve shifts to

higher temperatures, so the average reaction temperatures are increased. There, the endotherm becomes more pronounced (arrow “2” in Figure 8), which indicates that dissolution becomes more dominant compared with precipitation.

We now consider the process of cluster dissolution as a function of time. In addition to the hardness reduction, DSC traces provide more but indirect information on the microstructural change (Figure 9). Here, we avoid discussing details such as which exact phase is promoted or suppressed but focus on the most elementary aspects of precipitation. To understand the change of the DSC trace caused by RA, we need to understand the course of the DSC trace in the unrefreshed state (broken line in Figure 9). This, as has been partially discussed above, is first a predominant cluster dissolution (endotherm 2, possibly coupled with weak precipitation) and then the major precipitation reactions (exotherm 3). The latter is influenced by the former since it contains also the reprecipitation of the formerly dissolved solutes. After RA, the initial status before linear heating in DSC is varied, which leads to a different course of DSC endotherms and exotherms. To depict such changes clearly, we calculate the difference between the trace after and before RA, see Figure 9b,d. As RA proceeds, it shows a rising exothermic differential peak *a* and a progressing endothermic differential peak *b*. There can be two reasons contributing to the exothermic differential peak *a*. First, the endothermic cluster dissolution during DSC is reduced as clusters have already been dissolved during RA. Second, as more free solutes are available after RA, precipitation can occur at lower temperatures during linear heating, even at the temperature where the previous dissolution trough was. This shift of precipitation to lower temperatures during DSC is also partly the reason for the endothermic differential peak *b*. Another possible reason for peak *b* is the precipitation during RA, which reduces s.s. One peculiarity related to the growth of peak *a* is that it is not proportionate in the high- and low-temperature



regimes. A clear two-stage behavior can be seen as RA proceeds, especially for low RA temperature (e.g., 230 °C), which shows that the low-temperature part of the peak (*a1*) first emerges when RA time is short, and as RA gets longer, *a1* gradually saturates and the high-temperature part *a2* arises. This suggests that cluster dissolution might not be uniform throughout the RA process. Clusters in the later stage of RA require a higher temperature to dissolve or will reprecipitate at a higher temperature during DSC heating. A plausible interpretation is that the clusters in our “expired” alloy states have different stabilities. The model of Pashley et al. predicts that the stability of clusters can be influenced by the time and temperature of pretreatment.<sup>[22]</sup> A higher temperature produces clusters with higher stability, such as reported by Kim et al. that clusters formed at 100 °C are more stable than those formed at 20 °C, thus causing less hardness reversion during RA.<sup>[23]</sup> In addition, Poznak et al. claimed that the stability of clusters is related to the Mg/Si ratio by analyzing the chemistry of the clusters before and after AA using atom probe tomography, with Mg-rich clusters found to be more stable than Si-rich clusters.<sup>[24]</sup> Si-rich clusters that dissolve before Mg-rich clusters were also argued by Madanat et al. to explain the discrepancies of hardness and electrical resistivity evolutions during NSA.<sup>[11]</sup> PA clusters also have a higher Mg/Si ratio than NA clusters in these two alloys.<sup>[25,26]</sup> Therefore, we propose that the Si-rich clusters formed predominantly during NA are dissolved first during RA, causing an overall exothermic signal difference *a1*. As RA is prolonged, this process gradually comes to an end, and the Mg-rich clusters, formed mainly during PA, are dissolved, which then gives rise to the signal *a2*. RA at a higher temperature accelerates the entire dissolution process, which is why such transition is only partially visible or not captured at all, such as for RA at 270 °C. An increased RA temperature also enlarges the maximum peak area of *a*, indicating that more clusters are dissolved. However, only the magnitude of *a2* is enlarged, implying that more Mg-rich clusters (presumably PA clusters) are dissolved. The height of *a1* is less impacted, which is understandable since most clusters are already dissolvable even at 230 °C due to a generally lower stability.

Cluster stability and its relationship with cluster composition can be supported by the fact that cluster dissolution is also influenced by alloy chemistry. At the same temperature, the achievable relative hardness reversion is notably higher in alloy AA6016 (Figure 2c). An almost full hardness reversion is observable for AA6016 subjected to RA at 270 °C. This shows that the clusters are easier to dissolve in commercial AA6016 than in AA6014.

An effective activation energy for cluster dissolution can be calculated from the shift of the dissolution peak position at various heating rates by displaying  $\ln(\Phi/T_i^2)$  versus  $1/T_i$ , where  $T_i$  is the temperature of the minimum and  $\Phi$  the heating rate.<sup>[27]</sup> The activation energy  $E_a$  can be then calculated from the slope of the linear fitting. Here, we choose only the high heating rates for linear fitting since at low heating rates, the dissolution is partially masked by simultaneous precipitation. As in DSC at a higher heating rate cluster dissolution is predominant and precipitation suppressed, dissolution can be considered as the first reaction during DSC heating with a minimal influence of precipitation. Activation energies of 0.46 and 0.76 eV are obtained for cluster dissolution in AA6016 and AA6014, respectively. The latter is

close to the one obtained for AA6061,<sup>[10]</sup> while the value for AA6016 is much lower. Therefore, the lower activation energy found in AA6016 alloy might be the reason for the higher reversion ability of clusters.

#### 4.2.2. Precipitation

Precipitation during RA is in general undesired since it hardens an alloy and is normally accompanied by a loss of ductility, both complicate sheet forming. It consumes the s.s. which can be seen in the shrinking exothermic peaks (Figure 9a,c). The reduced s.s. reduces PB hardening, read in Section 4.3.1. Therefore, understanding precipitation during RA helps to determine the processing window of refreshment. Although precipitation relative to cluster dissolution is more suppressed at a higher aging temperature its absolute rate is enhanced due to increased thermal activation, thus shortening the time to reach a hardness minimum and the duration of the hardness trough, which narrows the processing window. The hardening effect of the precipitates formed at a higher RA temperature is lower, as seen by the hardening rate of AA6016 at 270 °C which is lower than at 250 °C, as well as the overaging stage observed for 290 °C in AA6014 is not seen for RA at lower temperatures. Precipitation during RA is faster and stronger in alloy AA6014 than AA6016, which can be attributed to two reasons: first, the AA6014 alloy used in this study has a stronger inherent age-hardening potential than the AA6016 as evidenced by the higher hardness in both direct PB and “expired” states, see Figure 2, possibly because the alloy composition is more balanced, which leads to stronger AA hardening than in either Si-rich or Mg-rich alloys.<sup>[28]</sup> Second, the higher stability of the clusters in AA6014 gives rise to less cluster dissolution at the same RA condition. The remaining clusters are presumably stable and might transform into larger precipitates, thus resulting in faster precipitation.

### 4.3. Reprecipitation after Refreshment

#### 4.3.1. PB Hardening

It has been demonstrated that both the absolute PB hardness and the PB hardness increase can be improved by applying suitable RA treatment, see Figure 2, which indicates that the solutes released from the dissolved clusters during RA lead to the formation of more hardening precipitates during PB than that in the unrefreshed sample. In AA6016, this partially reverts the “negative effect” caused by prolonged NA, while in AA6014 this yields a PB hardness even higher than that of the “fresh” sample. This suggests that there are already some deleterious clusters in the “fresh” state of AA6014, which are either due to the low PA temperature used or the NA included in the industrial processing procedure.

Solute atoms liberated from dissolving clusters are consumed if precipitation occurs at RA temperature, which can lower the thermodynamic driving force for precipitation during PB. These precipitates can still contribute to some hardening and, therefore, the final PB hardening can be roughly viewed as a competition between the hardening by the precipitates formed during RA and formed during PB.

### 4.3.2. NSA Stability

Reprecipitation of solutes from the dissolved clusters occurs also during NSA, but compared to AA, it relies more on the excess vacancies.<sup>[29]</sup> Madanat et al. modeled the kinetics of NSA after RA as a function of the s.s. and vacancy fraction evolutions during RA.<sup>[11]</sup> The kinetic factor, which is essentially a proxy of the rate constant describing the course of clustering after RA, is schematically represented in **Figure 10**, with the first climb due to the increased s.s. and vacancy site fraction, and the following drop attributed to the precipitation-related s.s. reduction. The hardness increment is monotonically related to the clustering rate constant. Our result of hardness increment after 50 days of NSA agrees well with the model, see Figure 5. The hardness increments as a function of RA time for various RA temperatures shown in Figure 5 can be illustratively overlaid on the master curve in Figure 10 to fit into the various stages of the process. The kinetics of both vacancy and cluster evolutions during RA are enhanced by a higher aging temperature, therefore for the same aging time, RA at higher temperatures lies in a later stage in the course.

A pronounced difference is seen between the NSA stability of the two investigated alloys. Figure 4 shows that NSA stability is higher for AA6014 when the same RA condition is performed, see Section 3.1.3, which is related to the higher difficulty to dissolve the clusters in AA6014, as discussed in Section 4.2.1, which results in less solute replenishment in the matrix. Of particular interest is the case of RA270/10, where a similar hardness drop is obtained in AA6016 ( $\Delta = 21$  HBW) and AA6014 ( $\Delta = 20$  HBW), see Figure 4. Since the hardening of clusters is reported approximately proportional to solute fraction,<sup>[14,30]</sup> enhancements of s.s. in both alloys are close. However, the outcome of the two alloys is very distinct. Refreshed AA6016 experiences a marked hardening within NSA for 1 day, whereas only a slight hardness increment is seen on AA6014 only after NSA for 7 days, see purple lines in Figure 4. There might be a difference in the exact Mg and Si contents in the alloy, but it does not explain such a huge discrepancy between the two alloys, as previous studies have shown for NA of alloys with different Mg and Si contents.<sup>[28,31]</sup> Moreover, stronger hardening during subsequent PB is seen in

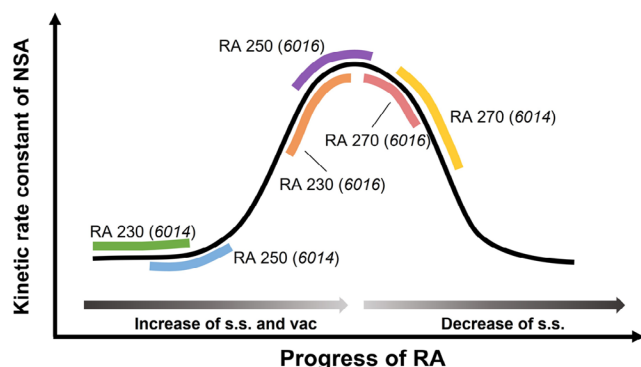


**Figure 10.** Schematic representation of the NSA kinetics versus progress of RA according to the study of Madanat et al.<sup>[11]</sup> and the overlay of hardness increments after 50 days of NSA from Figure 5.

AA6014, confirming that the remaining s.s. is at least not lower than in AA6016.

The key could lie in the mobile vacancies after RA. The vacancy dynamics simulation shows that the equilibrium vacancy concentration at 250 °C is reached within 15 s (dislocation density  $10^{11} \text{ m}^{-2}$ , jog fraction 0.02, grain size 50  $\mu\text{m}$ ).<sup>[21]</sup> At 270 °C, 10 s should be enough since the kinetics is much faster. However, what vacancy simulation does not include is the influence of solute clusters which can buffer the vacancy evolution due to a higher interaction energy.<sup>[29]</sup> As there are more undissolved clusters in AA6014, the buffering effect is stronger. Moreover, the dissolution of clusters also frees the vacancies imprisoned in them. A higher relative fraction of dissolution in AA6016 could free more vacancies. However, the trapped and freed vacancy concentration must be lower than  $7 \times 10^{-7}$ , because otherwise it would have been detected by positron annihilation lifetime measurements.<sup>[11]</sup> Another possible mechanism is the vacancy partitioning between the matrix and vacancy traps (clusters). This mechanism suggests that although the equilibrium vacancy concentration might have been reached at 270 °C, the repartition of vacancies between matrix and vacancy traps happens when the temperature is decreased to 20 °C, thus lowering the mobile matrix vacancy concentration.<sup>[29,32]</sup> More solute clusters have survived in AA6014 after RA, which could induce a stronger repartitioning effect. It is currently still unclear which mechanism is dominant, but what is in common among these mechanisms is that the remaining undissolved clusters play a pivotal role in controlling the mobile vacancy concentration after RA.

### 4.4. Industrial Refreshment Strategy for Expired Alloys

Refreshing the 6xxx alloys relies on dissolving the clusters formed during prior aging. However, this should not be the only criterion since higher RA temperatures or longer RA times, which usually promote more cluster dissolution, are found to induce more precipitation of less-hardening precipitates. Moreover, we found that undissolved clusters can be involved in controlling the mobile vacancy concentration, which helps to stabilize the alloy during NSA. In view of this, dissolution of some clusters, especially those formed during PA, seems undesired. Hence, the optimal refreshment window depends on the balance of these concerns, i.e., it should be carried out at a temperature as low as possible but as high as necessary, and for a time as short as possible but as long as necessary to dissolve undesired NA clusters. Using these criteria, the optimal processing window for the current alloys can be determined as (230–250 °C, 10–30 s) for alloy AA6016, and (250–270 °C, 5–20 s) for alloy AA6014. The processing window is dependent on the alloy composition, as it influences the thermal stability of the clusters. Generally, a higher temperature range should be used for clusters that are harder to dissolve, i.e., Mg-rich ones.

The effect of refreshment is sensitive to the highest RA temperature applied. Even minimum aging times in the current study (2 s, including 1 s for heating) lead to very pronounced differences in cluster reversion (Figure 2). However, refreshment experiments in various media demonstrate that refreshment is not sensitive to the heating rate in the range from 2.5 to

220 Ks<sup>-1</sup>, which indicates that the treatment is not sensitive to the history at lower temperatures. Instead, the soaking time at the maximum temperature matters most and should be counted. The fact that a high heating rate is not required facilitates industrial application.

Refreshment is easy to apply since only low temperatures and short times (compared with, e.g., solution heat treatment) are required. Therefore, it could be employed at the car manufacturer directly before forming, in which case NSA stability is not a concern. The serrations occurring in the tensile curve (Figure 7) should be considered since they might impact the surface quality after forming. Alternatively, refreshment can be employed at the aluminum producers. Here, NSA stability and its influence on the subsequent PB hardening have to be taken into consideration. It depends on the RA condition as well as on the alloy composition. We show that NSA can be further reduced by conducting PA, which can also enhance the PB hardness. We chose 80 °C for 20 h in our test, but other parameters, such as the normal PA used for the freshly solutionized and quenched alloy should in principle also work. In finding optimal treatment parameters, convenient hardness tests can replace the usual tensile tests for quick screening in the parameter space since an approximate linear relationship between yield strength ( $R_{p0.2}$ ) and hardness exists. Tensile tests are then merely needed to confirm results or to obtain elongation values.

## 5. Conclusion

We explored the feasibility of refreshing two commercial alloys, namely AA6016 and AA6014, that have naturally aged too long, here  $\approx 3.5$  years, and have lost their ability to reach sufficient strength during short AA, the so-called “paint baking (PB)”. We show that in such alloys, clusters can be reverted and PB hardness enhanced by applying a short aging treatment at a temperature between 230 and 290 °C for seconds up to a minute depending on the temperature. The following conclusions can be made: 1) RA leads to pronounced dissolution of clusters in the initial seconds of aging, after which precipitation sets in and increases hardness. Dissolution of clusters takes place in two stages, possibly in correlation with the Mg/Si ratio of the clusters. A higher temperature enables the dissolution of more clusters. 2) Clusters are more difficult to dissolve in AA6014 than in AA6016. RA at 270 °C can revert the hardness of the AA6016 close to the AQ state after solutionizing. An activation energy of 0.46 eV was found for cluster dissolution in AA6016, while the energy is 0.76 eV for AA6014. Therefore, a higher temperature is suggested for refreshing the AA6014 alloy. 3) Variation of the heating rate from 2.5 to 220 Ks<sup>-1</sup> has a minor effect on refreshment, indicating that RA is insensitive to some initial exposure to lower temperatures and the duration of soaking at the highest temperature should be considered instead of the overall heating time. 4) NSA after RA is influenced by the RA time and temperature, which agrees well with the model proposed by Madanat et al.<sup>[11]</sup> NSA also depends on the alloy composition. Alloy AA6014 is more stable against NSA than AA6016, which can be explained by the effect of vacancy trapping by the remaining undissolved clusters. PA can be performed on the refreshed alloys to further enhance NSA stability and PB hardening.

We expect that our refreshing strategy is applicable to other 6xxx alloys and also to alloys naturally aged longer than 3.5 years, since NA clustering progresses already very slowly after such a long storage.

## Acknowledgements

The authors would like to thank Dr. Tillmann Neu for the help in machining the tensile samples, Kathrin Matzak and Nadja Sonntag of Bundesanstalt für Materialforschung und -Prüfung (BAM) for the tensile testing, and Novelis Inc. for providing the material and the financial support.

Open Access funding enabled and organized by Projekt DEAL.

## Conflict of Interest

The authors declare no conflict of interest.

## Data Availability Statement

The data that support the findings of this study are available from the corresponding author upon reasonable request.

## Keywords

Al–Mg–Si alloys, clustering, natural aging, reversion

Received: July 19, 2023

Revised: September 27, 2023

Published online: October 27, 2023

- [1] J. Hirsch, *Trans. Nonferrous Met. Soc. China* **2014**, *24*, 1995.
- [2] J. Banhart, C. S. T. Chang, Z. Q. Liang, N. Wanderka, M. D. H. Lay, A. J. Hill, *Adv. Eng. Mater.* **2010**, *12*, 559.
- [3] J. Royset, T. Stene, J. A. Seater, O. Reiso, *Mater. Sci. Forum* **2006**, *519–521*, 239.
- [4] S. Pogatscher, H. Antrekowitsch, M. Werinos, F. Moszner, S. S. A. Gerstl, M. F. Francis, W. A. Curtin, J. F. Löffler, P. G. Uggowitzer, *Phys. Rev. Lett.* **2014**, *112*, 225701.
- [5] M. Werinos, H. Antrekowitsch, T. Ebner, R. Prillhofer, W. A. Curtin, P. J. Uggowitzer, S. Pogatscher, *Acta Mater.* **2016**, *118*, 296.
- [6] M. Liu, X. Zhang, B. Körner, M. Elsayed, Z. Liang, D. Leyvraz, J. Banhart, *Materialia* **2019**, *6*, 100261.
- [7] S. Muromachi, T. Mae, *Jpn. Inst. Met. Mater.* **1971**, *35*, 1021.
- [8] Z. Yang, Z. Liang, D. Leyvraz, J. Banhart, *Materialia* **2019**, *7*, 100413.
- [9] C. Haase, H. Wurst, *Z. Metallkd.* **1941**, *33*, 399.
- [10] S. Pogatscher, H. Antrekowitsch, H. Leitner, T. Ebner, P. J. Uggowitzer, *Acta Mater.* **2011**, *59*, 3352.
- [11] M. Madanat, M. Liu, J. Banhart, *Acta Mater.* **2018**, *159*, 163.
- [12] P. E. Fortin, *Met. Prog.* **1964**, *86*, 119.
- [13] Y. Birol, *Scr. Mater.* **2006**, *54*, 2003.
- [14] Z. Yang, I. Erdle, C. H. Liu, J. Banhart, *J. Mater. Sci. Technol.* **2022**, *120*, 78.
- [15] B. Milkereit, N. Wanderka, C. Schick, O. Kessler, *Mater. Sci. Eng. A* **2012**, *550*, 87.
- [16] Z. Yang, X. Jiang, X. Zhang, M. Liu, Z. Liang, D. Leyvraz, J. Banhart, *Scr. Mater.* **2021**, *190*, 179.
- [17] K. Strobel, M. D. H. Lay, M. A. Easton, L. Sweet, S. Zhu, N. C. Parson, A. J. Hill, *Mater. Charact.* **2016**, *111*, 43.

- [18] K. Strobel, M. A. Easton, M. D. H. Lay, P. A. Rometsch, S. Zhu, L. Sweet, N. C. Parson, A. J. Hill, *Metall. Mater. Trans. A* **2019**, 50A, 1957.
- [19] Z. Yang, X. H. Jiang, X. P. Zhang, M. Liu, Z. Q. Liang, D. Leyvraz, J. Banhart, in *ICAA17 Proc.*, Vol. 326, MATEC Web of Conferences, Grenoble, France **2020**, p. 02005.
- [20] Z. Yang, Z. Liang, D. Leyvraz, J. Banhart, *Data Brief* **2019**, 27, 104494.
- [21] F. Schmid, P. Dumitraschkewitz, T. Kremmer, P. J. Uggowitzer, R. Tosona, S. Pogatscher, *Commun. Mater.* **2021**, 2, 58.
- [22] D. W. Pashley, M. H. Jacobs, J. T. Vietz, *Philos. Mag.* **1967**, 16, 139.
- [23] J. Kim, S. Kim, E. Kobayashi, T. Sato, *Mater. Trans.* **2014**, 55, 768.
- [24] A. Poznak, R. K. W. Marceau, P. G. Sanders, *Mater. Sci. Eng. A* **2018**, 721, 47.
- [25] O. Engler, C. D. Marioara, Y. Aruga, M. Kozuka, O. R. Myhr, *Mater. Sci. Eng. A* **2019**, 759, 520.
- [26] D. Tweddle, J. A. Johnson, M. Kapoor, I. Bikmukhametov, S. Mileski, J. E. Carsley, G. B. Thompson, *Materialia* **2022**, 26, 101567.
- [27] E. J. Mittemeijer, *J. Mater. Sci.* **1992**, 27, 3977.
- [28] Y. Yan, *Ph.D. Thesis*, Technische Universität Berlin, **2014**.
- [29] Z. Yang, J. Banhart, *Acta Mater.* **2021**, 215, 117014.
- [30] M. J. Starink, L. F. Cao, P. A. Rometsch, *Acta Mater.* **2012**, 60, 4194.
- [31] S. N. Kim, J. H. Kim, E. Kobayashi, T. Sato, *Mater. Trans.* **2014**, 55, 1647.
- [32] M. F. Francis, W. A. Curtin, *Acta Mater.* **2016**, 106, 117.